Applied Catalysis B: Environmental 304 (2022) 121004

Contents lists available at ScienceDirect

Applied Catalysis B: Environmental

journal homepage: www.elsevier.com/locate/apcatb

Visible-light-driven semihydrogenation of alkynes via proton reduction over carbon nitride supported nickel

Tongtong Jia [a,b], Di Meng [a,b], Hongwei Ji [a,b], Hua Sheng [a,b], Chuncheng Chen [a,b], Wenjing Song [a,b,*], Jincai Zhao [a,b]

[a] Key Laboratory of Photochemistry, CAS Research/Education Center for Excellence in Molecular Sciences, Institute of Chemistry, Chinese Academy of Sciences, Beijing 100190, PR China

[b] University of Chinese Academy of Sciences, Beijing 100049, PR China

ARTICLE INFO

Keywords:
Alkyne semihydrogenation
Photocatalysis
Nickel catalysis
Metal-support synergy interaction

ABSTRACT

Semihydrogenation of alkynes represents one of the most viable route to produce functional alkene products. Herein we describe the visible-light-driven alcohol or water donating semihydrogenation catalyzed by nickel supported on carbon nitride scaffold (Ni/C_3N_4) under ambient condition, exhibiting excellent alkene selectivity and broad substrate scope. The catalyst design takes advantage of C_3N_4 to harvest visible irradiation and to tune the interaction of Ni with hydrogenation intermediates, which is essential for the excellent selectivity toward alkene products. The hydrogen atom incorporated in alkene products originates from hydroxyl group of methanol or water, via a Ni catalyzed proton reduction by photogenerated electrons to give the active surface hydrogen species (H*). Such hydrogenation pathway not only avoids harsh reaction condition but also enables facile synthesis of valuable deuterated alkenes using deuterated alcohols or D_2O, promising enormous application potential for well-designed catalyst architectures in the light-driven selective transfer hydrogenation (deuteration) of alkynes and other organic substrates.

1. Introduction

Functional alkenes are important building blocks in fine chemicals, pharmaceuticals and agrochemicals [1]. Semihydrogenation of alkynes represents an effective approach to produce alkene products [2,3]. The challenges for this reaction lies in the energy-demanding formation of active hydrogen species (e.g. by H_2 activation) and the effective depression of overhydrogenation to alkane by-products [4,5]. In the highly developed semihydrogenation by H_2 using either the classic Lindlar catalyst or other metal based catalysts, formation of H* (via H-H bond cleavage) often requires high temperature or pressure, which is energy intensive and brings safety concerns [6–9]. Other catalysts were also designed for transfer hydrogenation under milder condition using hydrides (silane, borohydride, and borane ammonia) [10–12], alcohols [13,14], formic acid [15,16], or water [17] as the hydrogen source. In these systems, however, elevated temperature, metal reductants, sophisticated metal ligands or other organic additives was still necessary, and the potential environmental risk and synthetic cost shall be considered [18].

Empowered by light, photocatalysis can sustainably drive energy demanding reactions by photogenerated carriers. Specifically, the proton reduction by conduction band electron, can be coupled to transfer hydrogenation, enabling environmental friendly, even waste-free semihydrogenation reaction [19,20]. Hitherto, most photocatalytic protocols relied on noble metal/alloy cocatalysts or UV irradiation [21–24], e.g., TiO_2 supported copper, platinum oxides, and eosin Y/Pd nanoparticles. Under photocatalytic condition, the semihydrogenation of alkyne might be interfered by the competitive hydrogen evolution or overhydrogenation, particularly at high conversion degree of alkyne substrate, which severely affected the purity of alkene products [24]. To alleviate these issues, Xiong et al. employed an alloying strategy, using PdPt alloy (supported on TiO_2) at a proper ratio to gain the balanced H* desorption/diffusion kinetics, depressing the overhydrogenation and hydrogen evolution reaction [23]. Mechanistic studies further suggested that light-driven hydrogenation does not mediated by the in situ formed H_2 gas (if there was any) since the alkene selectivity dropped when external H_2 was introduced under these conditions [22,23].

Polymeric carbon nitride (C_3N_4) scaffolds are appealing visible-light

* Corresponding author at: Key Laboratory of Photochemistry, CAS Research/Education Center for Excellence in Molecular Sciences, Institute of Chemistry, Chinese Academy of Sciences, Beijing 100190, PR China.
E-mail address: wsongunc@iccas.ac.cn (W. Song).

https://doi.org/10.1016/j.apcatb.2021.121004
Received 5 October 2021; Received in revised form 4 December 2021; Accepted 6 December 2021
Available online 10 December 2021

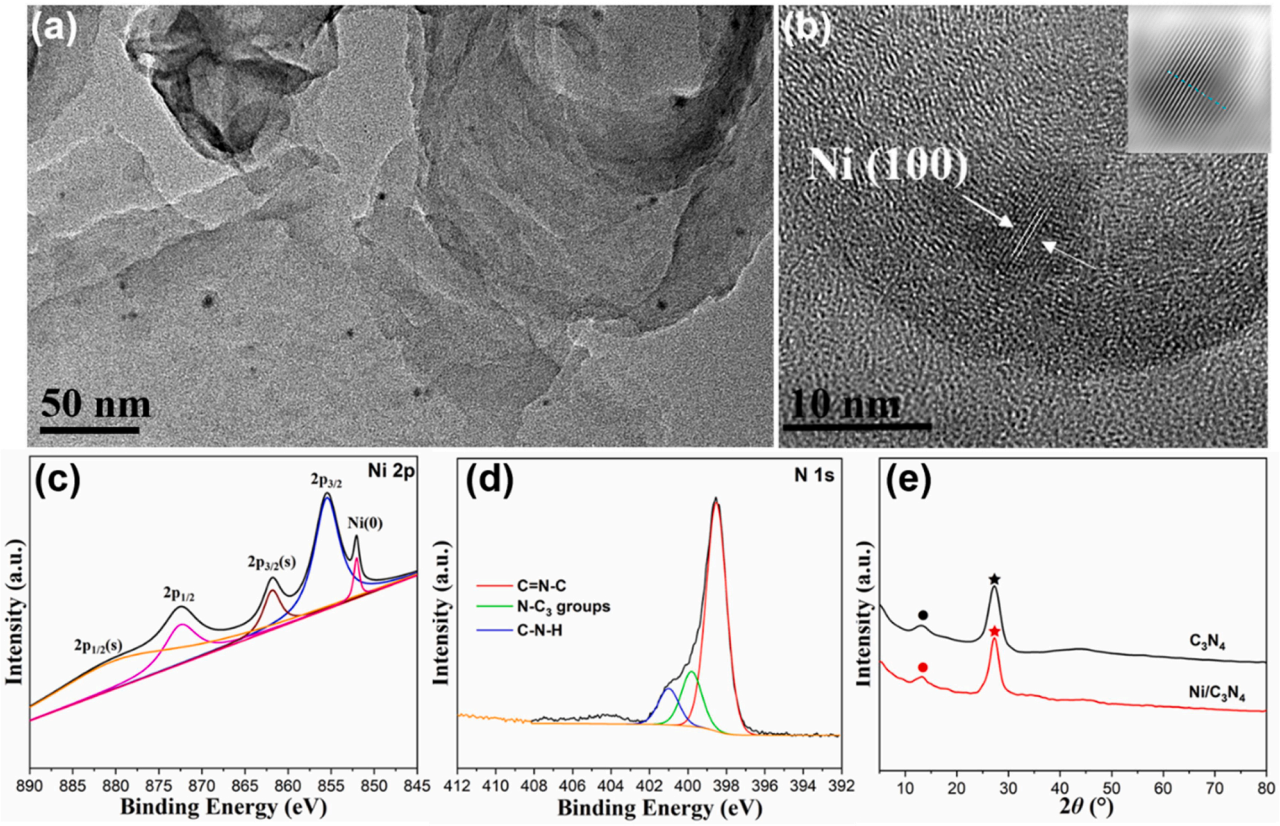

Fig. 1. Morphological and structural characterizations of Ni/C_3N_4. (a) HR-TEM image of Ni/C_3N_4 visualizing Ni nanoparticles. (b) Ni lattice fringes with the corresponding fast Fourier transform (FFT) as the inset. (c) Ni 2p and (d) N 1 s XPS spectra of Ni/C_3N_4. (e) XRD pattern of Ni/C_3N_4 and C_3N_4.

Table 1
Photocatalytic semihydrogenation of phenylacetylene under various conditions[a].

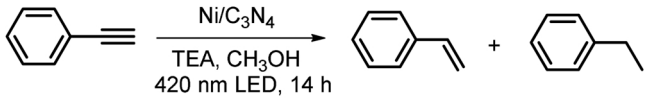

1 a 1 b 1 c

Entry	Condition variations	Conversion of **1a** (%)	Yield of **1b** (%)	Yield of **1c** (%)
1	None	100	97	n.d.
2	dark	none	n.d.	n.d.
3	No Ni/C_3N_4	none	n.d.	n.d.
4	C_3N_4 instead of Ni/C_3N_4	none	n.d.	n.d.
5	No TEA	26	24	n.d.
6	CH_3CN instead of CH_3OH	40	38	n.d.
7[b]	Ni/TiO_2	28	23	2.5
8	$Ni/ZnIn_2S_4$	none	n.d.	n.d.

[a] Standard conditions: 0.03 mmol phenylacetylene (1 equiv), 0.15 mmol TEA (5 equiv), 3 mg catalyst, 6 mL methanol as solvent, 420 nm LED irradiation (180 $mW{\cdot}cm^{-2}$). All reaction was carried out at 298 K under Ar atmosphere.
[b] Irradiation was provided by a Xenon arc lamp equipped with a 340 nm longpass filter.

photocatalyst with narrow bandgap and tunable band position to drive multiple redox transformations, including hydrogen production, CO_2 reduction, and organic pollutants degradation [25,26]. Moreover, C_3N_4 framework provide unique host environment for metal catalyst, affecting the electronics of the hosted metals and their interaction with substrates/intermediates which potentially benefit the activity/selectivity in light-driven alkyne semihydrogenation. Herein, we report C_3N_4 supported earth-abundant nickel catalyzed highly selective semihydrogenation of alkyne to alkene using methanol or water as the hydrogen (deuterium) source. DFT calculation suggests that C_3N_4 diminishes the affinity of alkenes (hydrogenation intermediates) to the supported Ni, and the process is kinetically favored in comparison to overhydrogenation. Importantly, hydrogen atoms incorporated in alkene products were derived from hydroxyl group via in situ formed metallic Ni mediated proton reduction by photogenerated electrons. Guided by such semihydrogenation pathway, deuterated alkenes, including the valuable pharmaceutical intermediates (e.g., methyl 4-pentenoate-[D_3]) were successfully synthesized with high deuterium incorporation from readily available CH_3OD or D_2O and unlabeled alkyne substrates [27,28].

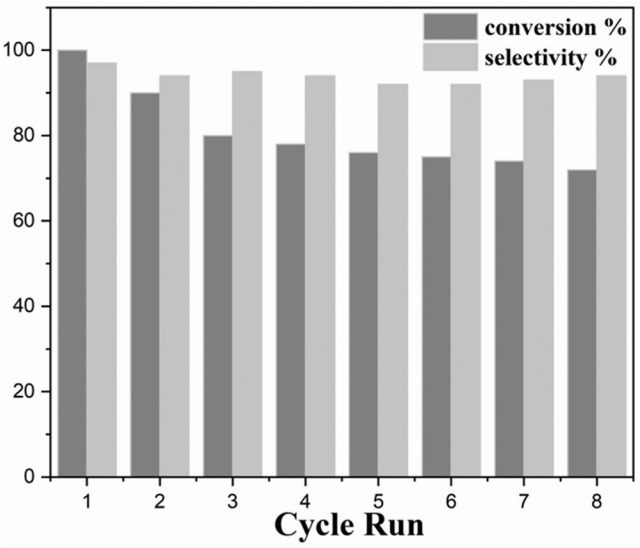

Fig. 2. Conversion of phenylacetylene and selectivity of styrene in eight consecutive catalytic runs using recycled Ni/C_3N_4 under standard reaction.

2. Experimental

2.1. Catalyst preparation and characterization

C_3N_4 was prepared by a slightly modified high-temperature thermal polymerization method according to the previously literatures [29,30]. Typically, 25 g urea was placed in a ceramic crucible with a cover and was transferred into a muffle furnace. The sample was heated to 550 °C for 2 h under air atmosphere. After cooling down to room temperature, light yellow solid was obtained.

Ni/C_3N_4 was synthesized by a $NaBH_4$ reduction method. First 100 mg C_3N_4 powder was dispersed into 20 mL $Ni(NO_3)_2.6\ H_2O$ aqueous solution which contains 0.25 mg Ni. Then the mixture was stirred for 30 min, followed by dropwise addition of $NaBH_4$ (5.8 mg in 5 mL DI water) to reduce Ni^{2+} to metallic Ni under continuous stirring (10 min reaction). After that, the centrifuged precipitate was washed with deionized water for two times and vacuum-dried at 60 °C overnight. The Ni loading level ranged from 0.14 to 1.05 wt%. Ni/C_3N_4 with 0.32 wt% Ni showed the best semihydrogenation performance and was used throughout the study unless otherwise noted (Table S1). Preparation process of TiO_2, or $ZnInS_4$ supported nickel were provided in the Supplementary material.

X-ray diffraction (XRD) was conducted on an X-ray diffractometer (Rigaku, Japan) with Cu- Kα radiation at a scan rate of 2° /min. Scanning electron microscopy (SEM) images were obtained with an SU8010 microscope (Hitachi, Japan). The UV–vis diffuse-reflection spectra (DRS) were recorded on a UV–vis spectrophotometer (HITACHI UH-4150). X-ray photoelectron spectroscopy (XPS) was conducted on a photoelectron spectrometer (ESCALAB250XI) with a Mg Kα (1253.6 eV) source. All binding energies were calibrated against the C1s peak at 284.8 eV. High-resolution transmission electron microscopy (HRTEM) images were obtained on JEM-2100 F microscope (JEOL, Japan) at an acceleration voltage of 200 kV. The Tecnai F20 energy-dispersive X-ray (EDX) spectrometer was equipped for elemental mapping of selected areas. Surface areas were obtained on a QUADRASORB automatic surface analyzer (Quantachrome, America) by the Brunauer-Emmett-Teller (BET) method. The Fourier transform infrared (FTIR) spectra were recorded on a BRUKER TENSOR-27 FT-IR spectrometer. Ni contents of catalysts were quantified by an inductively coupled plasma mass spectrometry (ICP-MS) (7700X). Steady state fluorescence spectra were recorded on PL spectrophotometer (HITACHI F7000). In situ electron paramagnetic resonance (EPR) spectra of the reaction suspension were measured using a Bruker E500 spectrometer at 77 K.

2.2. Photocatalytic semihydrogenation and product analysis

In a typical photo-reaction, Ni/C_3N_4 (3.0 mg) was dispersed in 6 mL methanol solution containing 0.03 mmol alkyne substrate and 0.15 mmol TEA (5 equiv). The photocatalytic reaction was carried out in Pyrex vessel with a water-circulating glass jacket to keep the temperature at 298 K. The reaction was carried out in (Ar) with 100 W 420 nm LED irradiation. Prior to irradiation, the suspensions were stirred in the dark for 30 min and was purged by Ar to remove air. At given time intervals, 0.2 mL of the suspension was filtered using 0.22 μm filter membrane, and the supernatant was sampled for GC-MS analysis, thin-layer chromatography (TLC), and NMR analysis.

Products were quantified on an Agilent 7890 gas chromatograph with a flame ionization detector (GC-FID) equipped with a HP-5 column (30 m × 320 μm × 0.25 μm) using calibration curves of the standards. Thin layer chromatography was carried out on SIL G/UV254 silica-aluminum plates and plates were visualized using ultra-violet light (254 nm) and $KMnO_4$ solution. ^{1}H NMR spectra of the isolated transfer hydrogenation products (dissolved in CD_3OD or $CDCl_3$) were recorded on a 300 MHz or 400 MHz Bruker Avance spectrometer. Reference chemical shift of solvent were taken as $\delta = 7.27$ ($CDCl_3$) and $\delta = 3.31$ (CD_3OD) for ^{1}H NMR. Multiplicities for coupled signals were designated using the following abbreviations: s = singlet, d = doublet, t = triplet, q = quartet, quin = quintet, br = broad signal, and are given in Hz.

2.3. Density functional theory (DFT) calculations

Density functional theory implemented in the Vienna Ab-initio Simulation Package (VASP) was employed to optimize the geometry of model catalyst [31,32]. The exchange-correlation interactions were described by the generalised gradient approximation (GGA) [33] in the form of the Perdew-Burke-Ernzerhof functional (PBE) [34]. A cut-off energy of 500 eV for plain-wave basis sets was adopted and the convergence threshold was 10^{-5} eV, and 5×10^{-3} eV/Å for energy and force, respectively. The weak interaction was described by DFT+D_3 method using empirical correction in Grimme's scheme [35]. The vacuum space was set to be more than 15 Å, which was sufficient to avoid the interaction between periodical images. Ni/C_3N_4 was modelled by a tetrahedral Ni_4 cluster with three Ni bonding to the pyridinic N of three heptazine unit in C_3N_4 supercell in reference to a previously published C_3N_4 supported Cu_4 cluster [36]. Bare tetrahedral Ni_4 cluster without support was also modeled for comparison. The minimum energy pathway for hydrogen migration was determined by using a climbing image nudged elastic band method (CINEB) [37,38].

3. Results and discussions

3.1. Catalyst structure analysis

Transmission electron microscopy (TEM) images of Ni/C_3N_4 (0.32 wt %) revealed homogeneously distributed Ni nanoparticles (~7 nm) (Fig. 1a). The lattice fringe of 0.318 nm corresponds to (110) plane of metallic Ni (Fig. 1b) [39–41]. The corresponding elemental mapping resolved the scattered nickel species in the matrix of carbon and nitrogen (Fig. S1). Scanning electron microscopy (SEM) images suggested that Ni/C_3N_4 composite is mainly composed of stacked irregular flakes

Table 2
Substrate scope of Ni/C_3N_4 catalyzed semihydrogenation.[a]

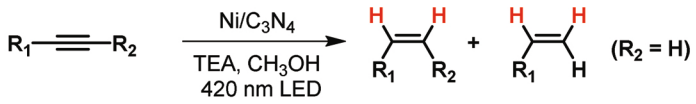

Entry	Substrate	Product	Time (h)[b]	Yield (%)[c]	
				Alkenes	Alkanes
1[d]	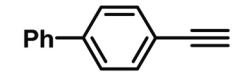	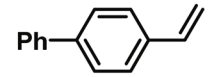	11	89	n.d.
2[d]	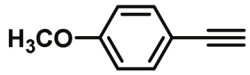	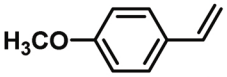	15	84	n.d.
3[d]	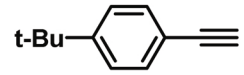	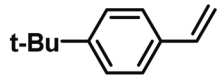	12	92	n.d.
4	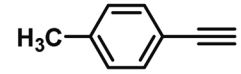	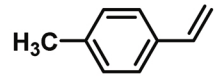	15	91	n.d.
5	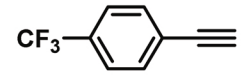	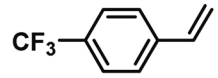	16	92	n.d.
6	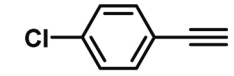	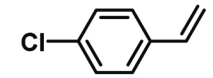	13	94	n.d.
7[d]	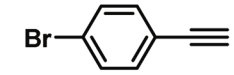	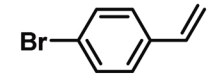	10	91	n.d.
8	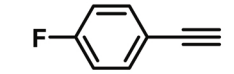	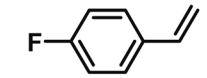	19	89	n.d.
9	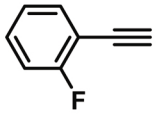	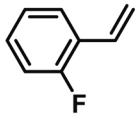	17	93	n.d.
10[d]	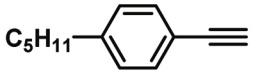	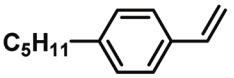	17	96	n.d.
11	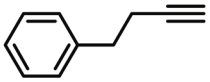	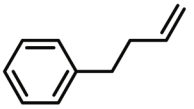	22	92	n.d.
12	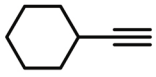	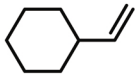	23	95	n.d.
13[d]	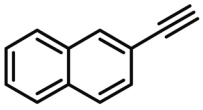	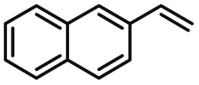	18	92 (84)	n.d.
14	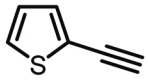	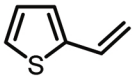	14	88	n.d.
15[e]	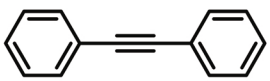		30	85 (Z/E=86/14)	n.d.
16[d,f,g]	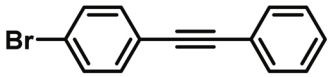	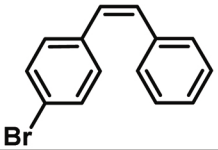	26	87 (Z/E=82/18)	n.d.

[a] Reaction conditions: alkyne substrates (0.03 mmol), Ni/C_3N_4 (3 mg), TEA (0.15 mmol), CH_3OH (6 mL), irradiation at 420 nm and 298 K under Ar. n.d. = not detected.
[b] reaction time at 100% conversion unless otherwise noted.

[c] GC yield.
[d] Isolated yield.
[e] 90% conversion.
[f] 95% conversion.
[g] 0.2 mmol substrate, 72% isolated yield.

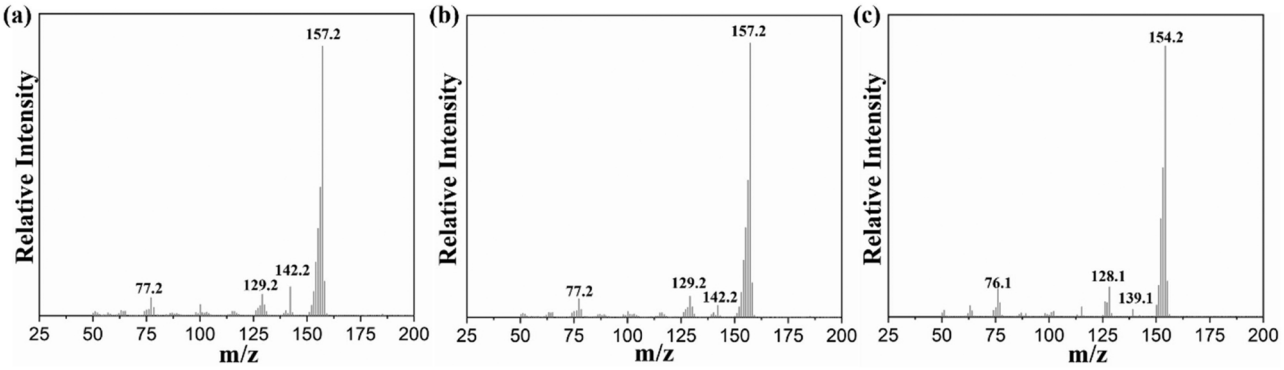

Fig. 3. Mass spectra of products (a) 2-vinylnaphthalene-[D_3] (3b) with 3 D atoms ($m/z = 157.2$), (b) 2-vinylnaphthalene-[D_3] (3b) with 3 D atoms ($m/z = 157.2$), and (c) 2-vinylnaphthalene without D atoms ($m/z = 154.2$) obtained in CH_3OD, CD_3OD, and CD_3OH, respectively. The isotopic labelling experiments are performed under standard reaction conditions. The NMR spectra for 2-vinylnaphthalene-[D_3] are provided in Fig. S11.

(Fig. S2). Presence of metallic Ni was further supported by the binding energies of 852.0 eV (Ni^0 $2p_{3/2}$) observed on XPS; Ni(II) species (formed by aerobic oxidation of Ni^0) was also resolved by Ni $2p_{1/2}$ and Ni $2p_{3/2}$ peaks at 872.5 and 855.5 eV, together with the corresponding satellite peaks at 880.0 and 861.8 eV, respectively (Fig. 1c) [40,42]. The N 1 s spectrum exhibits deconvoluted peaks of pyridinic N (398.5 eV), quaternary N (399.8 eV), and uncondensed amine N (401.1 eV) (Fig. 1d) [40,43,44]. In sample containing higher Ni level (1.05 wt%), a new peak at 400.1 eV appeared, which was tentatively ascribed to pyridinic nitrogen that coordinates to Ni (Fig. S3) [45–47]. Ni/C_3N_4 showed X-ray diffraction pattern of interlayer stacking of the aromatic systems at 27.6° and the in-plane heptazine units at 13.1°, index to (002) and (100) planes of graphitic phase of C_3N_4 (Fig. 1e) [48]. The heptazine C(sp^2)-N stretching vibration at 1636 cm^{-1} was also observed by FT-IR spectra (Fig. S4) [49]. Ni decoration did not affect the absorption feature of C_3N_4 support, but inhibited the radiative charge recombination (Fig. S5-S6) [41]. The specific surface area of Ni/C_3N_4 was 32.1 m^2 g^{-1}, slightly lower than that of C_3N_4 (42.3 $m^2 \cdot g^{-1}$) (Fig. S7) [29].

3.2. Photocatalytic semihydrogenation

The photocatalytic semihydrogenation activity of Ni/C_3N_4 was evaluated using phenylacetylene (**1a**) as the model substrate and the results are summarized in Table 1 and Table S1. Under optimized condition (1 equiv of **1a** and 5 equiv of TEA in methanol, 0.5 $g \cdot L^{-1}$ Ni/C_3N_4), 100% conversion of **1a** with 97% yield of styrene (**1b**) was achieved with 14 h under 420 nm LED irradiation (entry 1, ethylbenzene (**1c**) was not detected), corresponding to a TON of ~180 assuming all atoms in Ni particle were involved in the reaction. The excellent semihydrogenation performance of Ni/C_3N_4 was further corroborated by the insignificant H_2 evolution, even in the absence of **1a** (Fig. S8), i.e., semihydrogenation is preferred over hydrogen evolution in our catalytic systems [50]. Photo-irradiation, C_3N_4 and Ni were indispensable for the production of styrene (entries 2–4). The decreased yield of **1b** in the absence of TEA or in aprotic solvent acetonitrile (entries 5 and 6) implies the importance of accumulated electrons and proton for the light-driven semihydrogenation (in CH_3CN, hydrogen atoms in the product derived from TEA, which releases proton upon oxidation by hole). TEA are better hole scavenger than triethanolamine or methanol under the current photocatalytic condition (Table S1, entries 7–8). Other inorganic semiconductor, such as TiO_2, or $ZnIn_2S_4$ supported metallic Ni gave unsatisfied alkyne conversion or alkene selectivity (entries 7–8). Taken together, Ni/C_3N_4 successfully mediates the visible-light-driven semihydrogenation with methanol as the dominant hydrogen source, and as the Ni host, C_3N_4 may play an important role in dictating the excellent selectivity, which will be discussed in detail in the following section.

An important application of selective semihydrogenation is to remove trace alkyne impurity in alkene feedstock (e.g., the amount of phenylacetylene in styrene should be lower than 10 ppm) [14,51]. To test the performance of Ni/C_3N_4 in removing trace alkyne impurity, a **1b**/**1a** (10^{-1} M/10^{-3} M) mixture was subjected to the current photocatalytic protocol (Scheme S1, (i)). To our delight, 2 h irradiation completed remove **1a** and no ethylbenzene (**1c**) was detected. Removal of aliphatic 1-hexyne (**2a**) in 1-hexene (**2b**) was also successful without formation of alkane (Scheme S1, (ii)). The heterogeneous nature of Ni/C_3N_4 allowed readily catalyst separation and reuse (Fig. 2). We noticed a ~ 20% decrease in **1a** conversion under the same irradiation time from the 1st to the 3rd catalytic cycles, the semihydrogenation performance sustained well in the following runs. Notably, the **1b** selectivity in each run throughout the test was above 92%. The activity drop in the recycling reaction runs was possibly caused by the partial Ni leaching (Ni level decreased to 0.22 wt% after eight catalytic runs).

The photocatalytic protocol exhibits good substrate scope (Table 2). Terminal aromatic alkynes with electron donating or withdrawing groups on the aromatic rings converted to the corresponding alkenes smoothly with good to excellent yield (84–96%, entries 1–10) without formation of alkanes. Impressively, the protocol is compatible with various functionalities prone to hydrogenation, including fluoro, chloro, bromo and trifluoromethyl, suggesting an excellent chemoselectivity of Ni/C_3N_4. The excellent performance of Ni/C_3N_4 holds in the hydrogenation of aliphatic terminal alkynes (entries 11 and 12), affording the

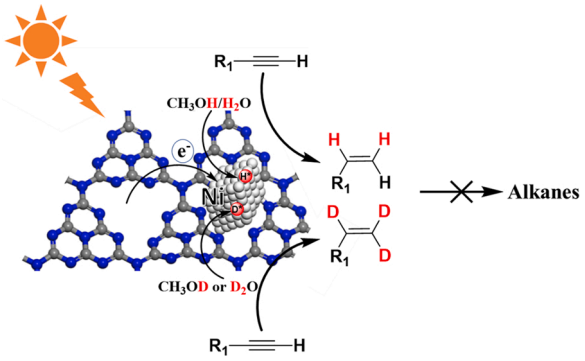

Scheme 1. Proposed reaction scheme for light-driven selective semihydrogenation of alkynes over Ni/C_3N_4, where the active hydrogen species was generated via reduction of (solvent) proton by photogenerated electrons, which then hydrogenate the alkyne substrates to give alkenes at high selectivity. Both proton reduction and semihydrogenation occur at the surface of supported Ni, catalyzed by metallic Ni (formed under in situ irradiation). Hole involved process is omitted for clarity. Balls in light grey, red, blue, and dark grey represents nickel, active hydrogen, nitrogen, and carbon atoms, respectively. (For interpretation of the references to colour in this figure, the reader is referred to the web version of this article.)

corresponding alkenes at yields above 90%. Polycyclic aromatic hydrocarbons 2-ethynylnaphthalene also underwent highly selective semihydrogenation, producing 2-vinylnaphthalene in 92% yield (entry 13). This compound was also tested for a larger scale reaction (30.4 mg, 0.2 mmol), producing 25.9 mg 2-vinylnaphthalene, corresponding to an isolated yield of 84% (entry 13, values shown in the parenthesis). Heterocyclic aromatic alkyne, 2-ethynylthiophene was also compatible with our photocatalytic protocol, giving 88% yield of 2-vinylthiophene (Table 2, entry 14). In addition, the semihydrogenation of internal alkynes, despite the need for an extended reaction time, demonstrated both high alkene yield (entries 15 and 16) and good stereo-selectivity towards the synthetically valuable cis-isomers (> 82%). A larger scale reaction (51.4 mg, 0.2 mmol) of 1-bromo-4-(phenylethynyl)benzene, also produced 37.3 mg (Z)-1-bromo-4-styrylbenzene, corresponding to 72% isolated yield (entry 16, condition g). The dominance of cis-isomer is usually observed in heterogeneous transfer hydrogenation. However, the energy transfers from the residue triplet excited states of carbon nitride (not quenched by Ni) to cis-alkenes might trigger the isomerization process. The light-driven, catalyst mediated isomerization was supported by the formation of 15% (E)-stilbene when subjecting (Z)-stilbene to our photocatalytic protocol (Scheme S2 and Fig. S9). Another possible pathway via an alkyl-Ni intermediate with rotatable C—C bond formed by addition of alkene to surface Ni-H* species [13,52], but this is beyond the scope of current study.

3.3. Photocatalytic semihydrogenation pathway and synthesis of deuterated alkenes

To gain further insight into the hydrogenation pathway and to fully exploit the advantage of the light-driven transfer hydrogenation, the reaction was performed in different deuterated methanol (CD_3OD, CD_3OH and CH_3OD), in the presence of TEA as the hole scavenger (Scheme S3). Starting from unlabelled 2-ethynylnaphthalene, 2-vinylnaphthalene-[D_3] with over 99% D incorporation was obtained in CH_3OD or CD_3OD (Fig. 3a and b). The original proton of the terminal -C≡C-H underwent TEA promoted exchange with solvent D (Scheme S3 and Fig. S10). It should be noted that H^+ would be released upon oxidation of TEA, however the concentration is too low (in comparison to the abundant D in deuterated methanol) to give appreciable H incorporation [53]. In CD_3OH, in contrast, D incorporation did not occur (Fig. 3c). Apparently, proton of the methanol hydroxyl group was the dominant hydrogen source. This is achieved by (methanol) proton reduction (by photogenerated electrons) at the surface of Ni cocatalyst [22,23], offering the active hydrogen species (H*) that are incorporated

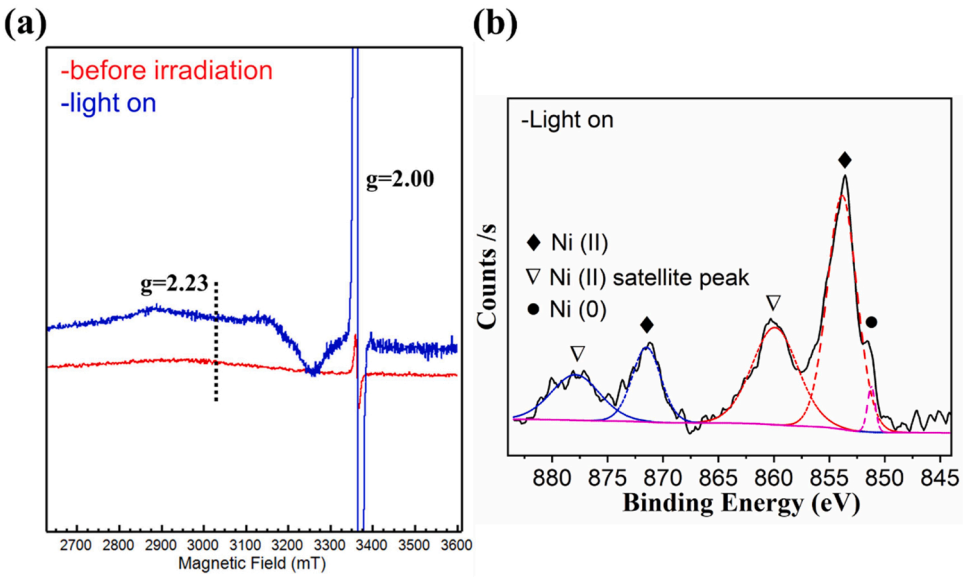

Fig. 4. (a) In situ EPR spectra obtained in suspensions of Ni/C_3N_4 (20 g L^{-1}) in methanol with 0.75 M TEA before and after 30 min 420 nm irradiation (200 mW·cm^{-2}). (b) In situ high-resolution Ni 2p XPS spectra of Ni/C_3N_4 under visible irradiation.

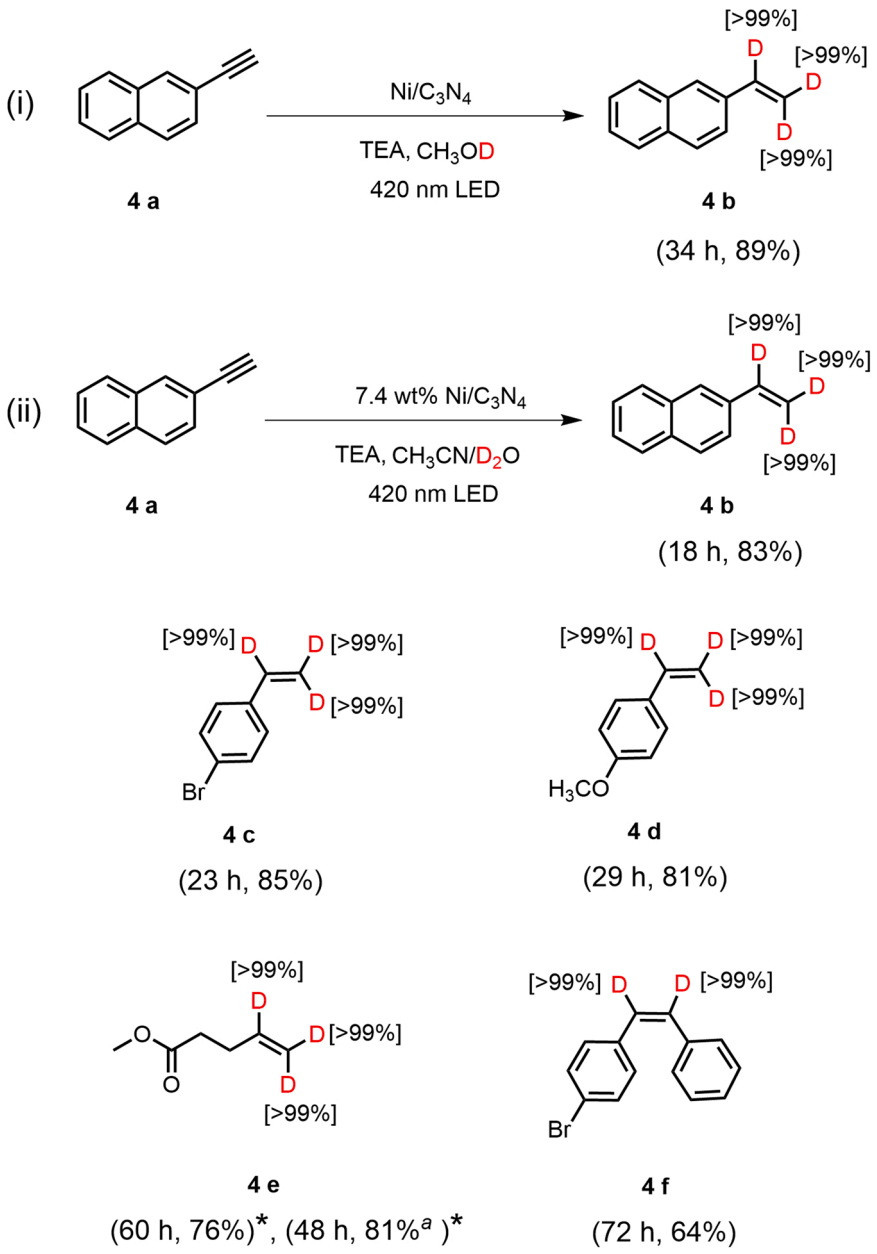

Scheme 2. Synthesis of deuterated alkenes. Isolated yield was reported unless otherwise noted. *GC yield. [a]Reaction in CH_3CN/D_2O.

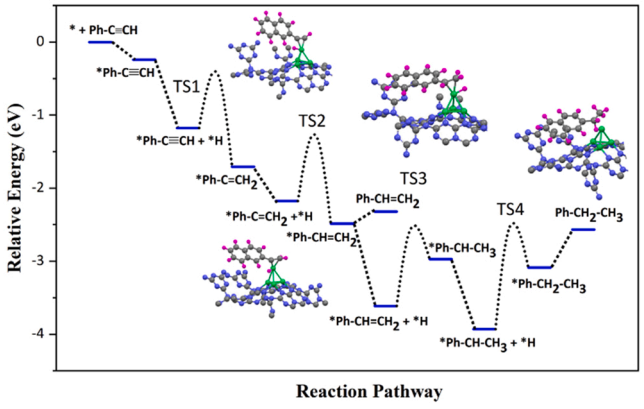

Fig. 5. DFT calculated hydrogenation energy barrier on Ni/C_3N_4, transition state configuration as shown inset. The pink, grey, blue, and green balls refer to H, C, N, and Ni atoms, respectively. (For interpretation of the references to colour in this figure, the reader is referred to the web version of this article.)

into alkene products (Scheme 1). In situ EPR measurement further revealed the in situ formation of metallic Ni species (g=2.23) (accompanied by accumulated electrons on C_3N_4 with a g value at 2.00) under visible irradiation (Fig. 4a) [42,54]. The photo-induced formation of metallic Ni was also supported by in situ XPS spectra (Fig. 4b), where the signal of Ni (0) as a shoulder peak at 851.22 eV was observed upon visible irradiation. Also, in comparison to XPS of the unirradiated Ni(II), there is a 0.6 eV shift to low binding-energy after visible irradiation, which suggests Ni(II) atoms could attract electrons from C_3N_4 planar layer (Fig. S12). Based on the observations in our study and previous investigations, the supported nickel nanoparticle mediates both formation of H* and the subsequent hydrogenation of the surface adsorbed alkynes; and the active state is metallic Ni which can form in situ under visible irradiation. Additionally, when TEMPO was added into the solution, conversion of phenylacetylene (**1a**) dropped to 30% (Table S1, entry 9), in line with a H* involved hydrogenation step.

Encouraged by the feasible D incorporation using CH_3OD, alkynes bearing various functionalities were subjected to our protocol. 2-

ethynylnaphthalene cleanly transformed to tri-deuterated 2-vinylnaphthalene products in CH_3OD with high deuterium incorporation (>99%) and good to excellent yields (Scheme 2, (i)). With the current photocatalytic protocol, transfer deuteration of 4-bromophenyacetylene afforded 4-bromostyrene-[D_3] without halogen-deuterium exchange, the undesired side-reaction observed in deuteration by using Na in EtOD-d_1 [28]. Valuable pharmaceutical intermediates (methyl 4-pentenoate-[D_3] was also produced at a yield of 76% with over 99% D incorporation. Furthermore, halogen substituted internal alkynes 1-bromo-4-(phenylethynyl)benzene also smoothly converted to the corresponding *cis*-alkenes-[D_2] without halogen-deuterium exchange or over-deuteration [28]. Importantly, the transfer deuteration can be translated to photocatalytic system employing low cost D_2O (CH_3CN: D_2O, v-v=4:1), producing tri-deuterated 2-vinylnaphthalene-[D_3] and (methyl 4-pentenoate-[D_3]at over 80% yield using catalyst Ni/C_3N_4 at 7.4 wt% Ni loading (Scheme 2, (ii)). The excellent selectivity and the controllable D-incorporation in the products undoubtedly highlight the potential of light-driven transfer semideuteration based on earth abundant materials and inexpensive deuterium sources [55–57].

3.4. Origin of the selectivity

To clarify the excellent selectivity of Ni/C_3N_4, the energy profile along the hydrogenation reaction coordinate was calculated using Density Functional Theory (DFT) employing periodic boundary conditions as implemented in the Vienna Ab-initio Simulation Package (VASP). Ni/C_3N_4 was modelled by a tetrahedral Ni_4 cluster with three Ni atom bonding to pyridinic N of three heptazine units of C_3N_4 supercell (Fig. 5 inset and Fig. S13-S17). As shown in Fig. 5, following the exoergic adsorption of 2-ethynylnaphthalene on top of the Ni cluster, consecutive addition of two H* adatom to 2-vinylnaphthalene are both thermodynamically downhill, with activation barriers of 0.82 eV (TS1) and 0.96 eV (TS2). The energy barrier for addition of another H* to form *Ph-CH-CH_3 intermediate is 1.13 eV (TS3), and this process is endothermic by 0.64 eV. In comparison, desorption of 2-vinyl naphthalene is more energy favoured ($\Delta G = 0.17$ eV), which is the key for the high alkene selectivity. The low affinity of alkene to Ni/C_3N_4 was also verified by independent alkyne/alkene adsorption tests (Fig. S18). In the absence of C_3N_4 as support, a significantly higher affinity of 2-vinyl naphthalene to Ni ($\Delta G = -1.86$ eV) was suggested by DFT calculation, which is expected to undergo kinetically feasible over-hydrogenation.

4. Conclusion

In summary, our study introduced a visible-light driven semi-hydrogenation protocol employing cost-effective and robust Ni/C_3N_4 catalyst to produce a variety of functional alkenes from alkynes using alcohol (water) as the hydrogen source. The photocatalytic protocol enjoys operation simplicity, low-cost and feasible catalyst recycle. C_3N_4 support was essential to tune the interaction of Ni and substrate/intermediate for the kinetically favoured alkene desorption over further-hydrogenation. This protocol was also viable for the synthesis of deuterium-labelled alkenes, including pharmaceutical product intermediate, using readily available deuterium source.

CRediT authorship contribution statement

Tongtong Jia: Experiments, Data collection, Writing – original draft. **Di Meng:** Methodology. **Hongwei Ji:** Methodology. **Hua Sheng:** Investigation, Methodology. **Chuncheng Chen:** Investigation, Methodology. **Wenjing Song:** Supervision, Methodology, Writing – review & editing, Project administration. **Jincai Zhao:** Supervision, Methodology, Writing – review & editing.

Declaration of Competing Interest

The authors declare that they have no known competing financial interests or personal relationships that could have appeared to influence the work reported in this paper.

Acknowledgements

This work was supported by the Strategic Priority Research Program of Chinese Academy of Sciences, Grant No. XDB36000000, National Natural Science Foundation of China (Nos. 21922609, 22076194, 21827809) and the "National Key Research and Development Program of China" (No. 2019YFA0210401, 2020YFA0710303).

Appendix A. Supporting information

Supplementary data associated with this article can be found in the online version at doi:10.1016/j.apcatb.2021.121004.

References

[1] Y. Kuwahara, H. Kango, H. Yamashita, Pd nanoparticles and aminopolymers confined in hollow silica spheres as efficient and reusable heterogeneous catalysts for semihydrogenation of alkynes, ACS Catal. 9 (2019) 1993–2006, https://doi.org/10.1021/acscatal.8b04653.
[2] C. Oger, L. Balas, T. Durand, J.-M. Galano, Are alkyne reductions chemo-, regio-, and stereoselective enough to provide pure (*Z*)-Olefins in polyfunctionalized bioactive molecules? Chem. Rev. 113 (2013) 1313–1350, https://doi.org/10.1021/cr3001753.
[3] R. Li, Y. Yue, Z. Chen, X. Chen, S. Wang, Z. Jiang, B. Wang, Q. Xu, D. Han, J. Zhao, Selective hydrogenation of acetylene over Pd-Sn catalyst: identification of Pd_2Sn intermetallic alloy and crystal plane-dependent performance, Appl. Catal. B: Environ. 279 (2020), 119348, https://doi.org/10.1016/j.apcatb.2020.119348.
[4] G. Vilé, D. Albani, N. Almora-Barrios, N. López, J. Pérez-Ramírez, Advances in the design of nanostructured catalysts for selective hydrogenation, ChemCatChem 8 (2016) 21–33, https://doi.org/10.1002/cctc.201501269.
[5] Y. Kuwahara, H. Yamashita, Design and synthesis of yolk–shell nanostructured silica encapsulating metal nanoparticles and aminopolymers for selective hydrogenation reactions, in: H. Yamashita, H. Li (Eds.), Core-Shell and Yolk-Shell Nanocatalysts, Springer, Singapore, 2021, pp. 395–411.
[6] R. Chinchilla, C. Nájera, Chemicals from alkynes with palladium catalysts, Chem. Rev. 114 (2014) 1783–1826, https://doi.org/10.1021/cr400133p.
[7] D. Albani, M. Shahrokhi, Z. Chen, S. Mitchell, R. Hauert, N. Lopez, J. Perez-Ramirez, Selective ensembles in supported palladium sulfide nanoparticles for alkyne semi-hydrogenation, Nat. Commun. 9 (2018) 2634, https://doi.org/10.1038/s41467-018-05052-4.
[8] S. Buchele, Z. Chen, E. Fako, F. Krumeich, R. Hauert, O.V. Safonova, N. Lopez, S. Mitchell, J. Perez-Ramirez, Carrier-induced modification of palladium nanoparticles on porous boron nitride for alkyne semi-hydrogenation, Angew. Chem. Int. Ed. 59 (2020) 19639–19644, https://doi.org/10.1002/anie.202005842.
[9] K. Choe, F. Zheng, H. Wang, Y. Yuan, W. Zhao, G. Xue, X. Qiu, M. Ri, X. Shi, Y. Wang, G. Li, Z. Tang, Fast and selective semihydrogenation of alkynes by palladium nanoparticles sandwiched in metal-organic frameworks, Angew. Chem. Int. Ed. 59 (2020) 3650–3657, https://doi.org/10.1002/anie.201913453.
[10] A.M. Whittaker, G. Lalic, Monophasic catalytic system for the selective semireduction of alkynes, Org. Lett. 15 (2013) 1112–1115, https://doi.org/10.1021/ol4001679.
[11] X. Wen, X. Shi, X. Qiao, Z. Wu, G. Bai, Ligand-free nickel-catalyzed semihydrogenation of alkynes with sodium borohydride: a highly efficient and selective process for cis-alkenes under ambient conditions, Chem. Commun. 53 (2017) 5372–5375, https://doi.org/10.1039/C7CC02140B.
[12] R. Kusy, K. Grela, Ligand-free (*Z*)-selective transfer semihydrogenation of alkynes catalyzed by in situ generated oxidizable copper nanoparticles, Green Chem. 23 (2021) 5494–5502, https://doi.org/10.1039/d1gc01206a.
[13] Z. Huang, Y. Wang, X. Leng, Z. Huang, An amine-assisted ionic monohydride mechanism enables selective alkyne cis-semihydrogenation with ethanol: from elementary steps to catalysis, J. Am. Chem. Soc. 143 (2021) 4824–4836, https://doi.org/10.1021/jacs.1c01472.
[14] G. Jaiswal, V.G. Landge, M. Subaramanian, R.G. Kadam, R. Zboril, M.B. Gawande, E. Balaraman, N-graphitic modified cobalt nanoparticles supported on graphene for tandem dehydrogenation of ammonia-borane and semihydrogenation of alkynes, ACS Sustain. Chem. Eng. 8 (2020) 11058–11068, https://doi.org/10.1021/acssuschemeng.9b07211.
[15] R. Kusy, K. Grela, E- and Z-selective transfer semihydrogenation of alkynes catalyzed by standard ruthenium olefin metathesis catalysts, Org. Lett. 18 (2016) 6196–6199, https://doi.org/10.1021/acs.orglett.6b03254.
[16] J.L. Fiorio, T.P. Araújo, E.C.M. Barbosa, J. Quiroz, P.H.C. Camargo, M. Rudolph, A. S.K. Hashmi, L.M. Rossi, Gold-amine cooperative catalysis for reductions and reductive aminations using formic acid as hydrogen source, Appl. Catal. B: Environ. 267 (2020), 118728, https://doi.org/10.1016/j.apcatb.2020.118728.

[17] C.-Q. Zhao, Y.-G. Chen, H. Qiu, L. Wei, P. Fang, T.-S. Mei, Water as a hydrogenating agent: stereodivergent Pd-catalyzed semihydrogenation of alkynes, Org. Lett. 21 (2019) 1412–1416, https://doi.org/10.1021/acs.orglett.9b00148.

[18] D. Wang, D. Astruc, The golden age of transfer hydrogenation, Chem. Rev. 115 (2015) 6621–6686, https://doi.org/10.1021/acs.chemrev.5b00203.

[19] K. Su, Y. Wang, C. Zhang, Z. Gao, J. Han, F. Wang, Tuning the Pt species on Nb_2O_5 by support-induced modification in the photocatalytic transfer hydrogenation of phenylacetylene, Appl. Catal. B: Environ. 298 (2021), 120554, https://doi.org/10.1016/j.apcatb.2021.120554.

[20] M. Navlani-García, P. Verma, D. Salinas-Torres, R. Raja, K. Mori, H. Yamashita, Single-site heterogeneous catalysts and photocatalysts for emerging applications. Advanced Heterogeneous Catalysts Volume 2: Applications at the Single-Atom Scale, American Chemical Society, 2020, pp. 151–188.

[21] J.J. Zhong, Q. Liu, C.J. Wu, Q.Y. Meng, X.W. Gao, Z.J. Li, B. Chen, C.H. Tung, L. Z. Wu, Combining visible light catalysis and transfer hydrogenation for in situ efficient and selective semihydrogenation of alkynes under ambient conditions, Chem. Commun. 52 (2016) 1800–1803, https://doi.org/10.1039/c5cc08697c.

[22] S. Imai, K. Nakanishi, A. Tanaka, H. Kominami, Accelerated semihydrogenation of alkynes over a copper/palladium/titanium(IV) oxide photocatalyst free from poison and H_2 Gas, ChemCatChem 12 (2020) 1609–1616, https://doi.org/10.1002/cctc.201902175.

[23] M. Li, N. Zhang, R. Long, W. Ye, C. Wang, Y. Xiong, PdPt alloy nanocatalysts supported on TiO_2: maneuvering metal-hydrogen interactions for light-driven and water-donating selective alkyne semihydrogenation, Small 13 (2017), https://doi.org/10.1002/smll.201604173.

[24] J. Lian, Y. Chai, Y. Qi, X. Guo, N. Guan, L. Li, F. Zhang, Unexpectedly selective hydrogenation of phenylacetylene to styrene on titania supported platinum photocatalyst under 385 nm monochromatic light irradiation, Chin. J. Catal. 41 (2020) 598–603, https://doi.org/10.1016/s1872-2067(19)63453-4.

[25] Y. Li, M. Gu, X. Zhang, J. Fan, K. Lv, S.A.C. Carabineiro, F. Dong, 2D g-C_3N_4 for advancement of photo-generated carrier dynamics: status and challenges, Mater. Today 41 (2020) 270–303, https://doi.org/10.1016/j.mattod.2020.09.004.

[26] X. Li, Z. Hu, Q. Li, M. Lei, J. Fan, S.A.C. Carabineiro, Y. Liu, K. Lv, Three in one: atomically dispersed Na boosting the photoreactivity of carbon nitride towards NO oxidation, Chem. Commun. 56 (2020) 14195–14198, https://doi.org/10.1039/D0CC05948J.

[27] A. Kurimoto, R.S. Sherbo, Y. Cao, N.W.X. Loo, C.P. Berlinguette, Electrolytic deuteration of unsaturated bonds without using D_2, Nat. Catal. 3 (2020) 719–726, https://doi.org/10.1038/s41929-020-0488-z.

[28] M. Han, Y. Ding, Y. Yan, H. Li, S. Luo, A. Adijiang, Y. Ling, J. An, Transition-metal-free, selective reductive deuteration of terminal alkynes with sodium dispersions and EtOD-d_1, Org. Lett. 20 (2018) 3010–3013, https://doi.org/10.1021/acs.orglett.8b01036.

[29] Y. Wang, X. Wang, M. Antonietti, Polymeric graphitic carbon nitride as a heterogeneous organocatalyst: from photochemistry to multipurpose catalysis to sustainable chemistry, Angew. Chem. Int. Ed. 51 (2012) 68–89, https://doi.org/10.1002/anie.201101182.

[30] X. Zhao, C. Deng, D. Meng, H. Ji, C. Chen, W. Song, J. Zhao, Nickel-coordinated carbon nitride as a metallaphotoredox platform for the cross-coupling of aryl halides with alcohols, ACS Catal. 10 (2020) 15178–15185, https://doi.org/10.1021/acscatal.0c04725.

[31] G. Kresse, J. Furthmüller, Efficient iterative schemes for ab initio total-energy calculations using a plane-wave basis set, Phys. Rev. B 54 (1996) 11169–11186, https://doi.org/10.1103/PhysRevB.54.11169.

[32] G. Kresse, J. Furthmüller, Efficiency of ab-initio total energy calculations for metals and semiconductors using a plane-wave basis set, Comput. Mater. Sci. 6 (1996) 15–50, https://doi.org/10.1016/0927-0256(96)00008-0.

[33] J.P. Perdew, K. Burke, M. Ernzerhof, Generalized gradient approximation made simple, Phys. Rev. Lett. 77 (1996) 3865–3868, https://doi.org/10.1103/PhysRevLett.77.3865.

[34] J.P. Perdew, M. Ernzerhof, K. Burke, Rationale for mixing exact exchange with density functional approximations, J. Chem. Phys. 105 (1996) 9982–9985, https://doi.org/10.1063/1.472933.

[35] S. Grimme, Semiempirical GGA-type density functional constructed with a long-range dispersion correction, J. Comput. Chem. 27 (2006) 1787–1799, https://doi.org/10.1002/jcc.20495.

[36] X. Bai, Q. Li, L. Shi, X. Niu, C. Ling, J. Wang, Hybrid Cu^0 and Cu^{x+} as atomic interfaces promote high-selectivity conversion of CO_2 to C_2H_5OH at low potential, Small 16 (2020), 1901981, https://doi.org/10.1002/smll.201901981.

[37] G. Henkelman, B.P. Uberuaga, H. Jónsson, A climbing image nudged elastic band method for finding saddle points and minimum energy paths, J. Chem. Phys. 113 (2000) 9901–9904, https://doi.org/10.1063/1.1329672.

[38] G. Henkelman, H. Jónsson, Improved tangent estimate in the nudged elastic band method for finding minimum energy paths and saddle points, J. Chem. Phys. 113 (2000) 9978–9985, https://doi.org/10.1063/1.1323224.

[39] Ö. Metin, V. Mazumder, S. Özkar, S. Sun, Monodisperse nickel nanoparticles and their catalysis in hydrolytic dehydrogenation of ammonia borane, J. Am. Chem. Soc. 132 (2010) 1468–1469, https://doi.org/10.1021/ja909243z.

[40] L. Kong, Y. Dong, P. Jiang, G. Wang, H. Zhang, N. Zhao, Light-assisted rapid preparation of a Ni/g-C_3N_4 magnetic composite for robust photocatalytic H_2 evolution from water, J. Mater. Chem. A 4 (2016) 9998–10007, https://doi.org/10.1039/C6TA03178A.

[41] C. Han, R. Zhang, Y. Ye, L. Wang, Z. Ma, F. Su, H. Xie, Y. Zhou, P.K. Wong, L. Ye, Chainmail co-catalyst of NiO shell-encapsulated Ni for improving photocatalytic CO_2 reduction over g-C_3N_4, J. Mater. Chem. A 7 (2019) 9726–9735, https://doi.org/10.1039/C9TA01061K.

[42] A. Indra, P.W. Menezes, K. Kailasam, D. Hollmann, M. Schröder, A. Thomas, A. Brückner, M. Driess, Nickel as a co-catalyst for photocatalytic hydrogen evolution on graphitic-carbon nitride (sg-CN): what is the nature of the active species? Chem. Commun. 52 (2016) 104–107, https://doi.org/10.1039/C5CC07936E.

[43] Q. Han, B. Wang, Y. Zhao, C. Hu, L. Qu, A graphitic-C_3N_4 "seaweed" architecture for enhanced hydrogen evolution, Angew. Chem. Int. Ed. 54 (2015) 11433–11437, https://doi.org/10.1002/anie.201504985.

[44] C. Sun, H. Zhang, H. Liu, X. Zheng, W. Zou, L. Dong, L. Qi, Enhanced activity of visible-light photocatalytic H_2 evolution of sulfur-doped g-C_3N_4 photocatalyst via nanoparticle metal Ni as cocatalyst, Appl. Catal. B: Environ. 235 (2018) 66–74, https://doi.org/10.1016/j.apcatb.2018.04.050.

[45] M. Shalom, D. Ressnig, X. Yang, G. Clavel, T.P. Fellinger, M. Antonietti, Nickel nitride as an efficient electrocatalyst for water splitting, J. Mater. Chem. A 3 (2015) 8171–8177, https://doi.org/10.1039/C5TA00078E.

[46] S. Ohn, S.Y. Kim, S.K. Mun, J. Oh, Y.J. Sa, S. Park, S.H. Joo, S.J. Kwon, S. Park, Molecularly dispersed nickel-containing species on the carbon nitride network as electrocatalysts for the oxygen evolution reaction, Carbon 124 (2017) 180–187, https://doi.org/10.1016/j.carbon.2017.08.039.

[47] A. Vijeta, C. Casadevall, S. Roy, E. Reisner, Visible-light promoted C–O bond formation with an integrated carbon nitride–nickel heterogeneous photocatalyst, Angew. Chem. Int. Ed. 60 (2021) 8494–8499, https://doi.org/10.1002/anie.202016511.

[48] X. Wang, K. Maeda, A. Thomas, K. Takanabe, G. Xin, J.M. Carlsson, K. Domen, M. Antonietti, A metal-free polymeric photocatalyst for hydrogen production from water under visible light, Nat. Mater. 8 (2009) 76–80, https://doi.org/10.1038/nmat2317.

[49] J. Fu, K. Liu, K. Jiang, H. Li, P. An, W. Li, N. Zhang, H. Li, X. Xu, H. Zhou, D. Tang, X. Wang, X. Qiu, M. Liu, Graphitic carbon nitride with dopant induced charge localization for enhanced photoreduction of CO_2 to CH_4, Adv. Sci. 6 (2019), 1900796, https://doi.org/10.1002/advs.201900796.

[50] H. Kominami, M. Higa, T. Nojima, T. Ito, K. Nakanishi, K. Hashimoto, K. Imamura, Copper-modified titanium dioxide: a simple photocatalyst for the chemoselective and diastereoselective hydrogenation of alkynes to alkenes under additive-free conditions, ChemCatChem 8 (2016) 2019–2022, https://doi.org/10.1002/cctc.201600290.

[51] D.S. Deng, Y. Yang, Y.T. Gong, Y. Li, X. Xu, Y. Wang, Palladium nanoparticles supported on mpg-C_3N_4 as active catalyst for semihydrogenation of phenylacetylene under mild conditions, Green Chem. 15 (2013) 2525–2531, https://doi.org/10.1039/c3gc40779a.

[52] K. Li, R. Khan, X. Zhang, Y. Gao, Y. Zhou, H. Tan, J. Chen, B. Fan, Cobalt catalyzed stereodivergent semi-hydrogenation of alkynes using H_2O as the hydrogen source, Chem. Commun. 55 (2019) 5663–5666, https://doi.org/10.1039/C9CC01970G.

[53] Y. Yabe, Y. Sawama, Y. Monguchi, H. Sajiki, Site-selective deuterated-alkene synthesis with palladium on boron nitride, Chem. Eur. J. 19 (2013) 484–488, https://doi.org/10.1002/chem.201203337.

[54] Y. Wei, Y. Gong, X. Zhao, Y. Wang, R. Duan, C. Chen, W. Song, J. Zhao, Ligand directed debromination of tetrabromodiphenyl ether mediated by nickel under visible irradiation, Environ. Sci. Nano 6 (2019) 1585–1593, https://doi.org/10.1039/C9EN00175A.

[55] K.T. Neumann, S. Klimczyk, M.N. Burhardt, B. Bang-Andersen, T. Skrydstrup, A. T. Lindhardt, Direct trans-selective ruthenium-catalyzed reduction of alkynes in two-chamber reactors and continuous flow, ACS Catal. 6 (2016) 4710–4714, https://doi.org/10.1021/acscatal.6b01045.

[56] L. Li, W. Yang, Q. Yang, Q. Guan, J. Lu, S.-H. Yu, H.-L. Jiang, Accelerating chemo- and regioselective hydrogenation of alkynes over bimetallic nanoparticles in a metal–organic framework, ACS Catal. 10 (2020) 7753–7762, https://doi.org/10.1021/acscatal.0c00177.

[57] Y. Chang, A. Yesilcimen, M. Cao, Y. Zhang, B. Zhang, J.Z. Chan, M. Wasa, Catalytic deuterium incorporation within metabolically stable β-Amino C–H bonds of drug molecules, J. Am. Chem. Soc. 141 (2019) 14570–14575, https://doi.org/10.1021/jacs.9b08662.